Supporting Information

Design of Novel Bismaleimide-Based Single-Ion Conducting Hybrid Electrolytes for High Ionic Conductivity and Extended Cycling Stability Lithium-Metal Batteries

Yu Ding[1], Shicheng Zhang[1], Xiao Wang, Puyan Huang, Yuwei Zhong, Jifang Fu*

Nano-Science & Technology Research Center, College of Sciences, Shanghai University, 99 Shangda Road, Shanghai 200444, PR China

.

Table S1. Composition of the polymer electrolyte membranes

Sample	Li-BMIBSI (g)	MAPOSS (g)	VEC (g)	PVDF-HFP (g)	POSS (wt %)
BMI-blank	1.92	0	0	1	0
P_0-BMI-SCPE	1.92	0	2.24	1	0
$P_{2.5}$-BMI-SCPE	1.92	0.1	2.24	1	2.5
P_5-BMI-SCPE	1.92	0.2	2.24	1	5
P_{10}-BMI-SCPE	1.92	0.4	2.24	1	10

* Corresponding author

Email address: fjfshu@hotmail.com or fjfshu@shu.edu.cn(JF. Fu)

[1] These authors contributed equally to this work.

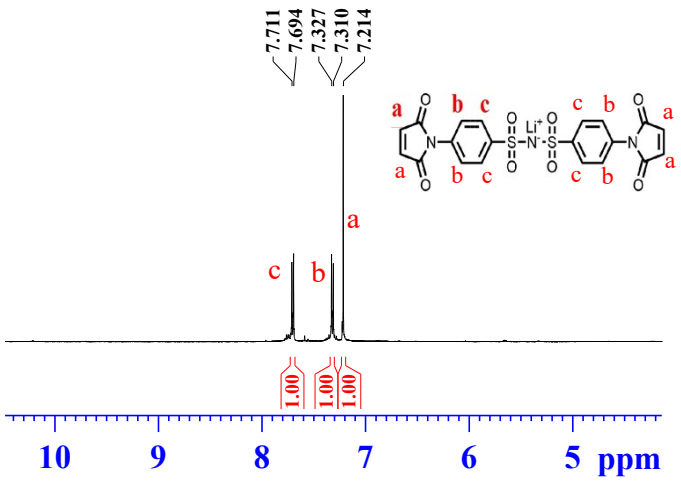

Figure S1. The ^{1}H NMR spectra of Li-BMIBSI.

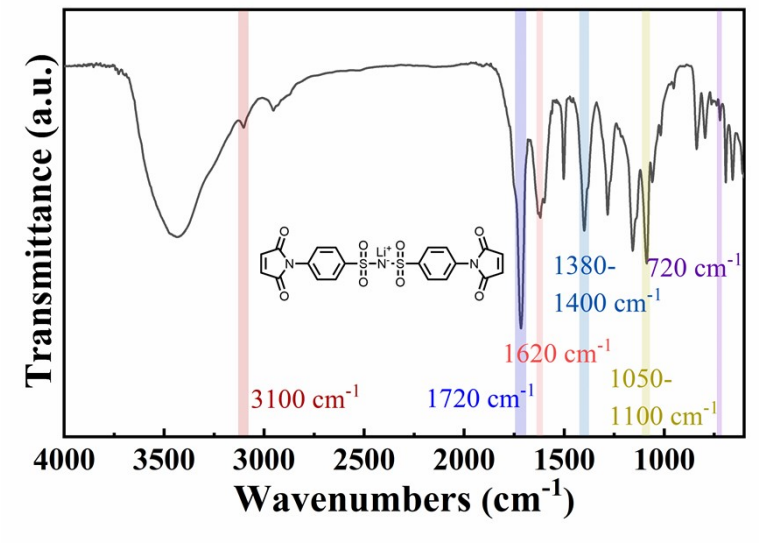

Figure S2. FTIR spectra of Li-BMIBSI.

Figure S3. Optical image of P_x-BMI-SCPEs.

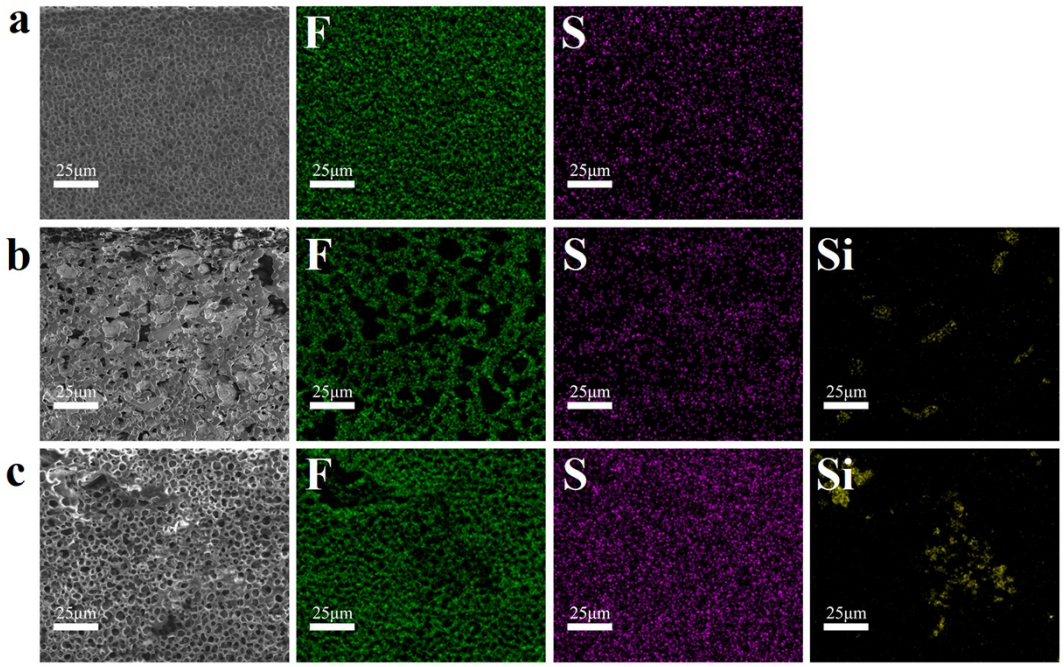

Figure S4. Surface SEM images of (a) P_0-BMI-SCPE, (b) $P_{2.5}$-BMI-SCPE, (c) P_{10}-BMI-SCPE, and its EDS element mapping of F, S, Si.

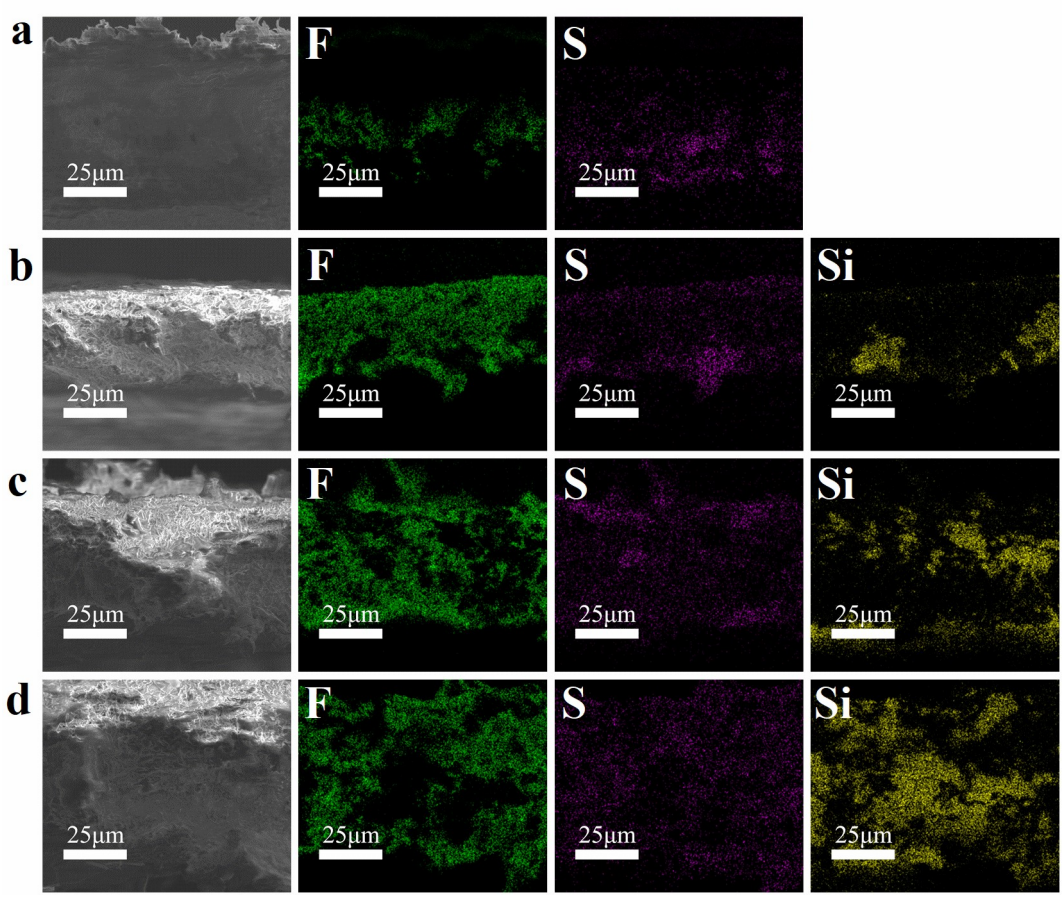

Figure S5. Cross-sectional SEM images of (a) P_0-BMI-SCPE, (b) $P_{2.5}$-BMI-SCPE, (c) P_5-BMI-SCPE, (d) P_{10}-BMI-SCPE, and its EDS element mapping of F, S, Si.

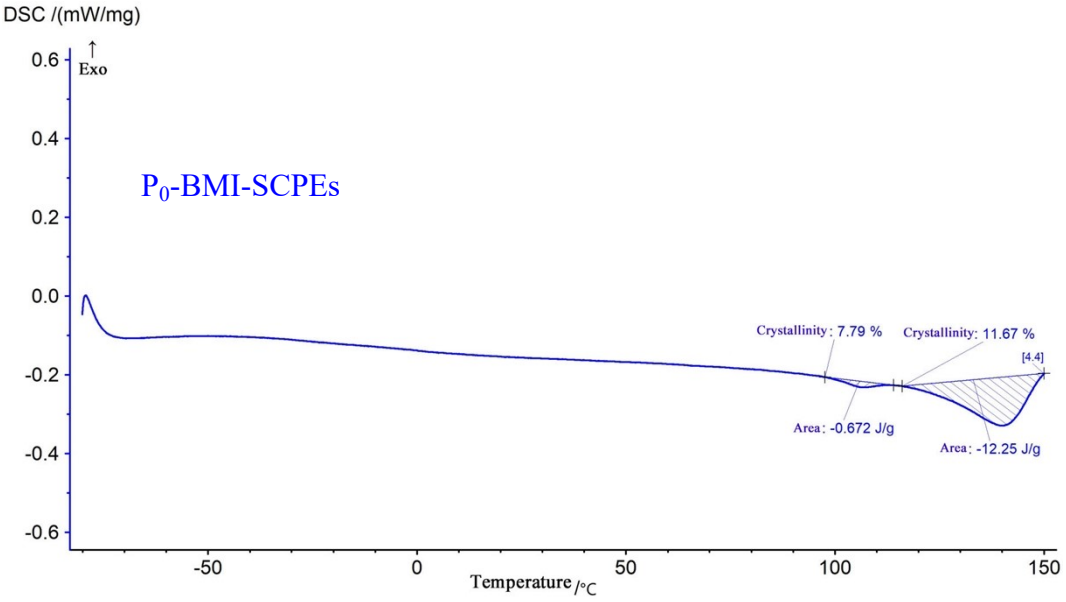
DSC /(mW/mg)
Exo
0.6
0.4
0.2
0.0
-0.2
-0.4
-0.6
P0-BMI-SCPEs
Crystallinity : 7.79 %
Crystallinity: 11.67 %
[4.4]
Area : -0.672 J/g
Area : -12.25 J/g
-50
0
50
100
150
Temperature /°C

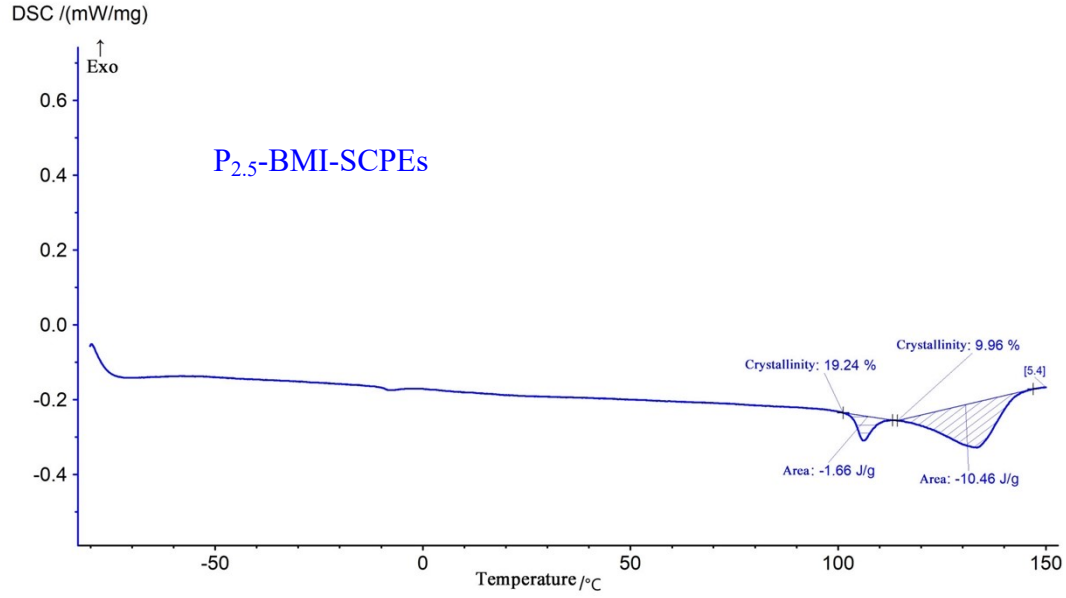
DSC /(mW/mg)
Exo
0.6
0.4
0.2
0.0
-0.2
-0.4
P2.5-BMI-SCPEs
Crystallinity: 9.96 %
Crystallinity: 19.24 %
[5.4]
Area : -1.66 J/g
Area : -10.46 J/g
-50
0
50
100
150
Temperature /°C

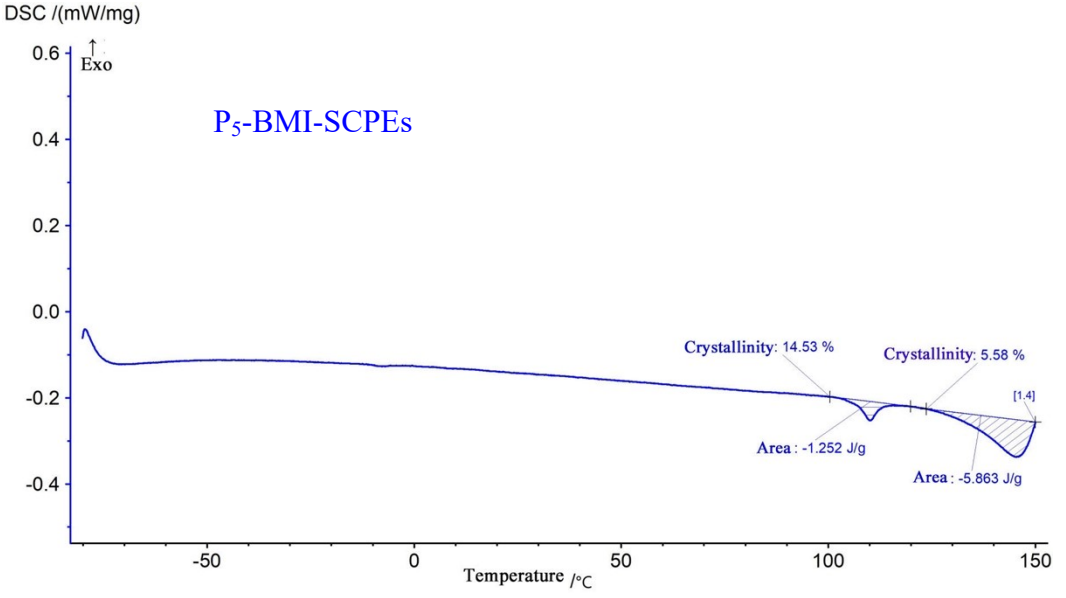
DSC /(mW/mg)
Exo
0.6
0.4
0.2
0.0
-0.2
-0.4
P5-BMI-SCPEs
Crystallinity: 14.53 %
Crystallinity: 5.58 %
[1.4]
Area : -1.252 J/g
Area : -5.863 J/g
-50
0
50
100
150
Temperature /°C

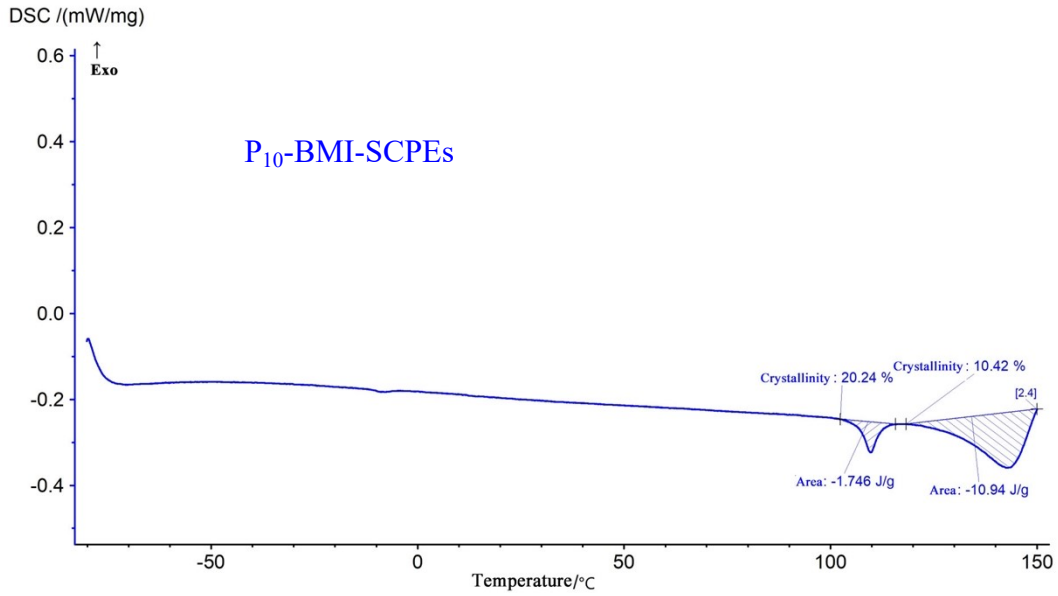

Figure S6. DSC curves and corresponding crystallinity of P_x-BMI-SCPEs in the range of -80 - 150 ℃

The crosslink density is test through tensile testing.

$$E \approx 3\rho RT$$

Here, E is Young's modulus, R is the universal gas constant (8.314 J mol^{-1} K^{-1}), and T is the absolute temperature.

Table S2. Crystallinity, Young's modulus, crosslink density and gel content of Px-BMI-SCPE

Sample	Crystallinity of P(LiBMIBSI) (%)	Crystallinity of PVDF-HFP (%)	Young's modulus (MPa)	crosslink density (ρ,mol/m^3)	electrolytes uptake （wt %）	gel content (wt%)
P_0-BMI-SCPE	7.79	11.67	1.02	137.16	76.736	56.58157
$P_{2.5}$-BMI-SCPE	19.24	9.96	1.07	143.88	53.125	65.30612
P_5-BMI-SCPE	14.53	5.58	1.43	192.30	105.227	48.72653
P_{10}-BMI-SCPE	20.24	10.24	1.25	168.09	24.405	80.38262

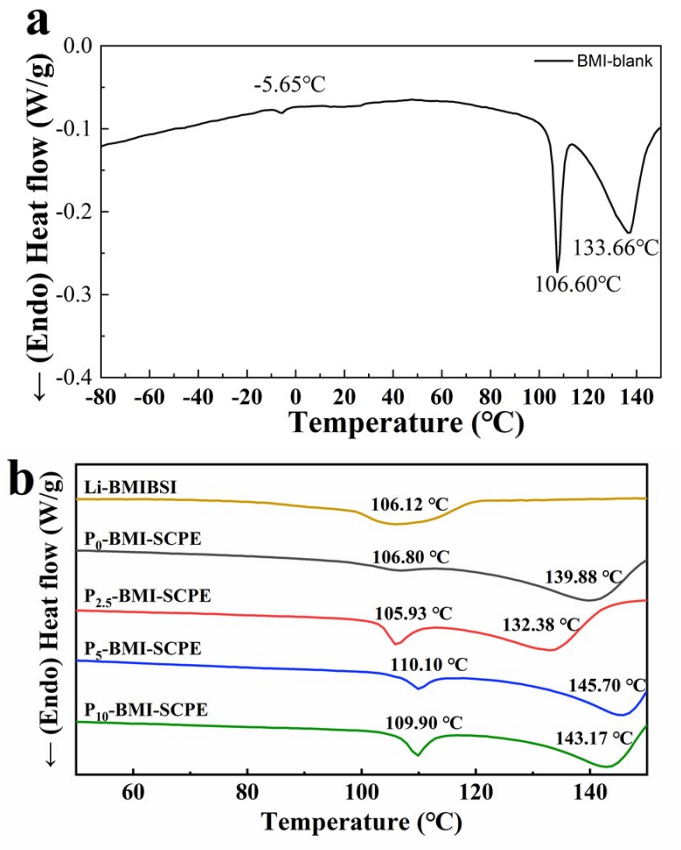

Figure S7. DSC curves of BMI-blank (a) and P_x-BMI-SCPEs and Li-BMIBSI (b) in the range of 50 - 150 ℃

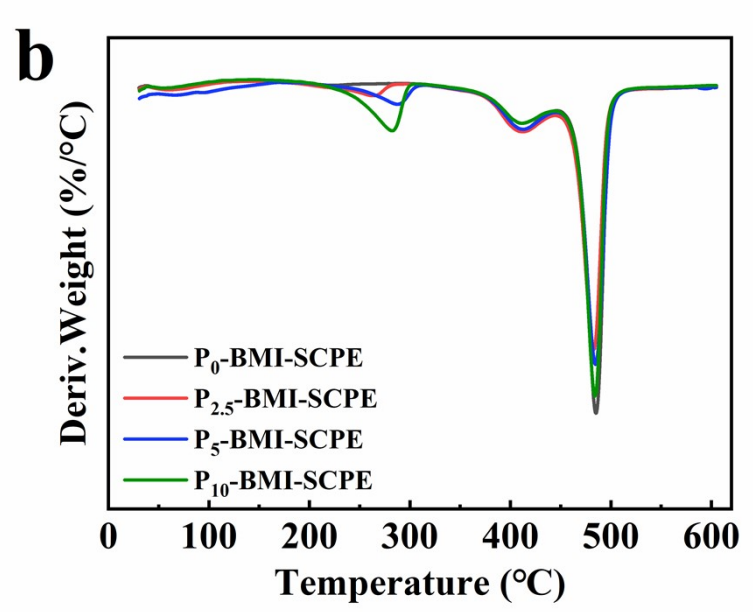

Figure S8. DTG curves of P_x-BMI-SCPEs.

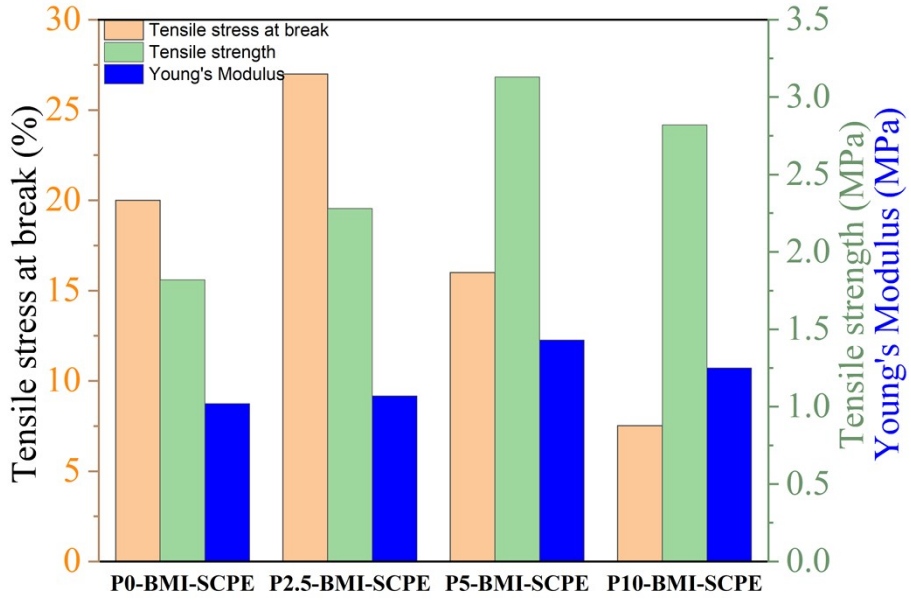

Figure S9. Tensile stress at break (%), tensile strength and Young's Modulus of P_x-BMI-SCPEs.

Table S3. Thermal stability of P_x-BMI-SCPEs

Sample	M_{PS} (%)	T_{PS}-0 (℃)	T_{PS}-max (℃)	T_{max1} (℃)	T_{max2} (℃)	Chard yield (%) at 600 ℃
P_0-BMI-SCPE				411.3	485.0	34.9
$P_{2.5}$-BMI-SCPE	4.2	231.4	263.8	412.4	482.8	34.9
P_5-BMI-SCPE	6.4	251.7	288.5	412.5	484.6	28.5
P_{10}-BMI-SCPE	11.0	249.2	282.1	411.6	484.2	30.9

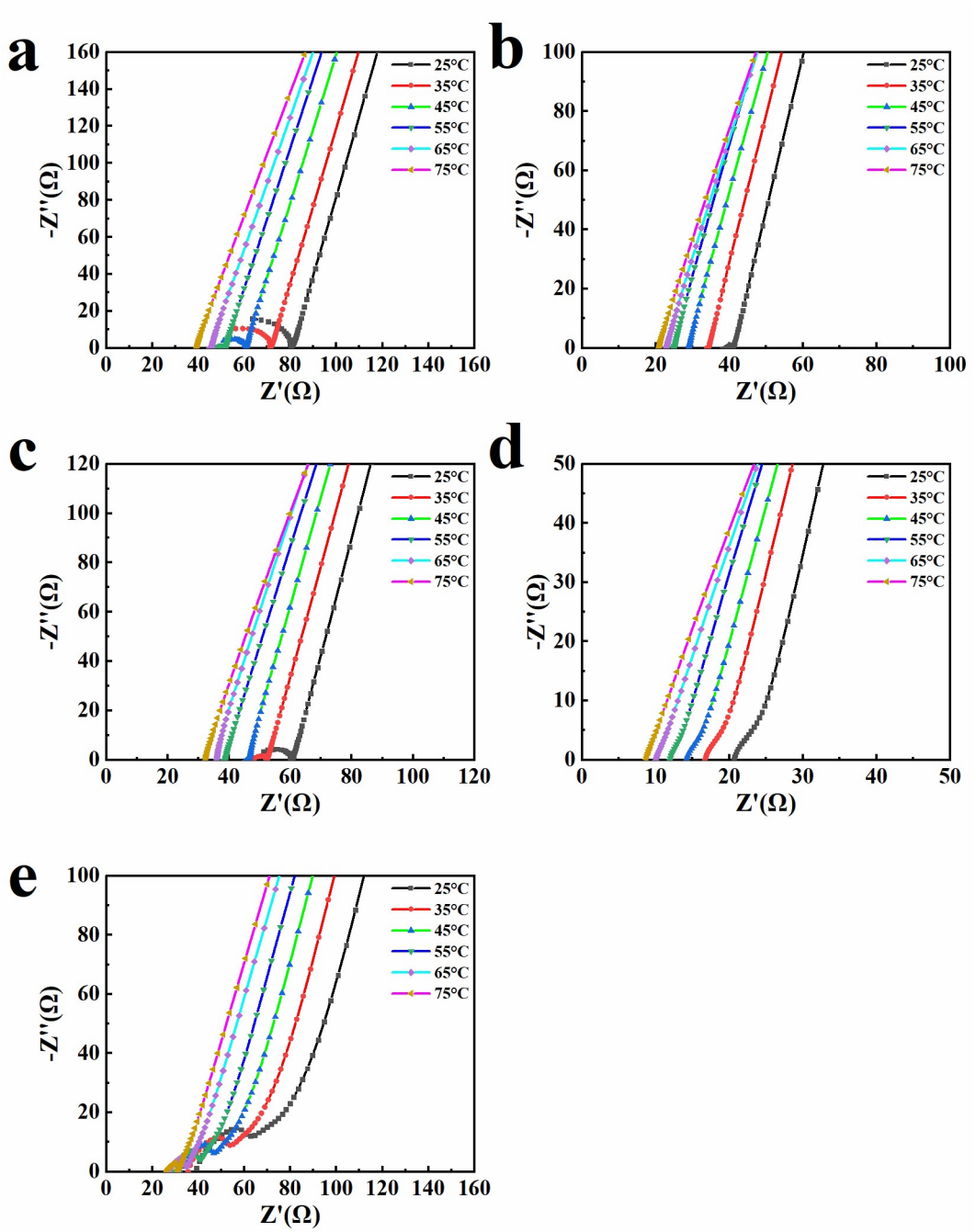

Figure S10. EIS impedance plots at different temperature for (a) BMI-blank, (b) P_0-BMI-SCPE, (c) $P_{2.5}$-BMI-SCPE, (d) P_5-BMI-SCPE, (e) P_{10}-BMI-SCPE.

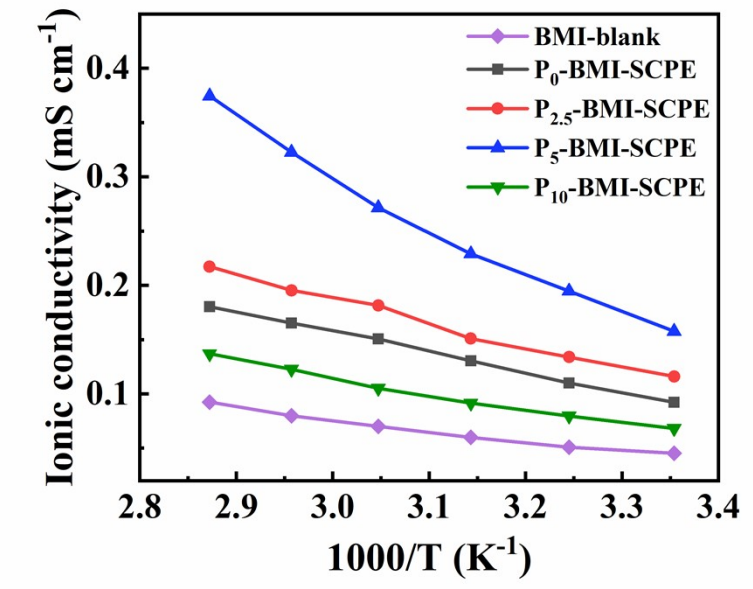

Figure S11**.** Temperature dependence of ionic conductivity of P_x-BMI-SCPEs and BMI-blank.

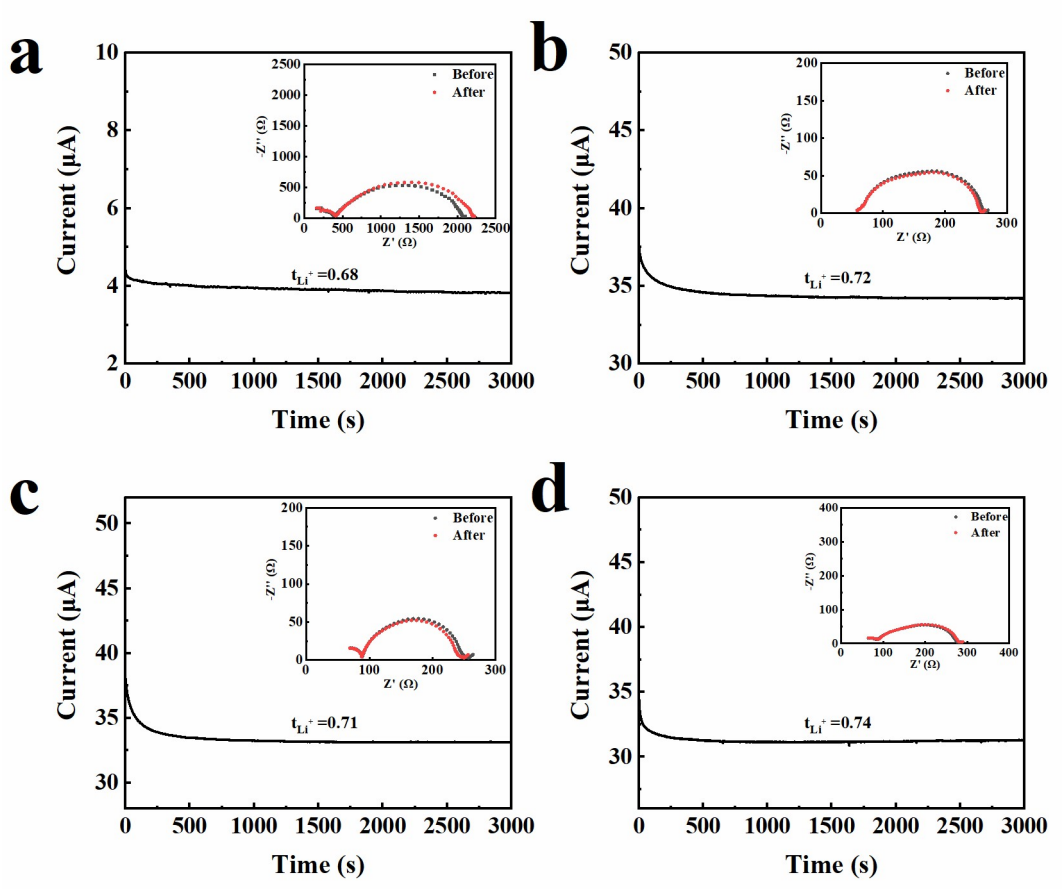

Figure S12. Polarization curves as well as the initial and steady-state impedance diagram of (a) symmetric Li|BMI-blank|Li cell, (b) symmetric Li|P_0-BMI-SCPE|Li cell, (c) symmetric Li|$P_{2.5}$-BMI-SCPE|Li cell, (d) symmetric Li|P_{10}-BMI-SCPE|Li cell.

Table S4. EIS and DC polarization results used to calculate t_{Li}^+ of PSCHEs

Sample	R_0 (Ω)	R_s (Ω)	I_0 (μA)	I_s (μA)	ΔV	t_{Li}^+
BMI-blank	1677	1795	4.47	3.83	0.01	0.68
P_0-BMI-SCPE	197.2	192.3	37.5	34.6	0.01	0.72
$P_{2.5}$-BMI-SCPE	169.1	162.2	38.1	34.0	0.01	0.71
P_5-BMI-SCPE	433.7	424.7	13.8	12.7	0.01	0.80
P_{10}-BMI-SCPE	194.2	197.3	35.2	31.3	0.01	0.74

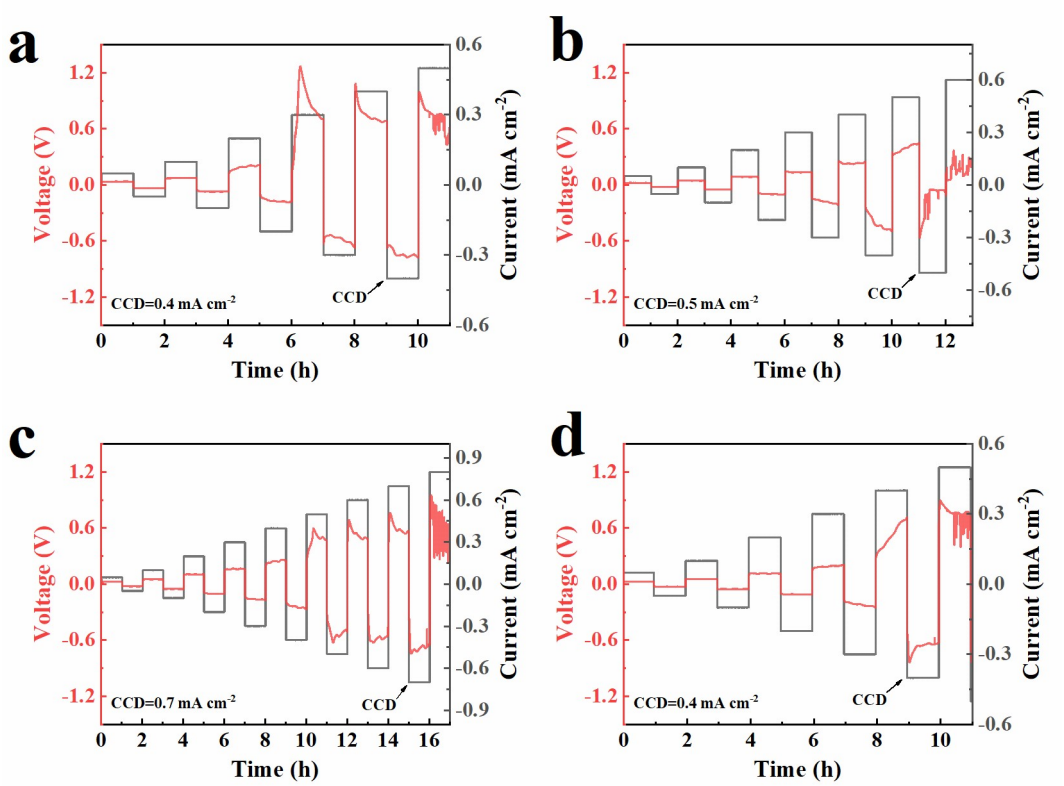

Figure S13. CCD curves of symmetric Li|P_x-BMI-SCPEs|Li cells

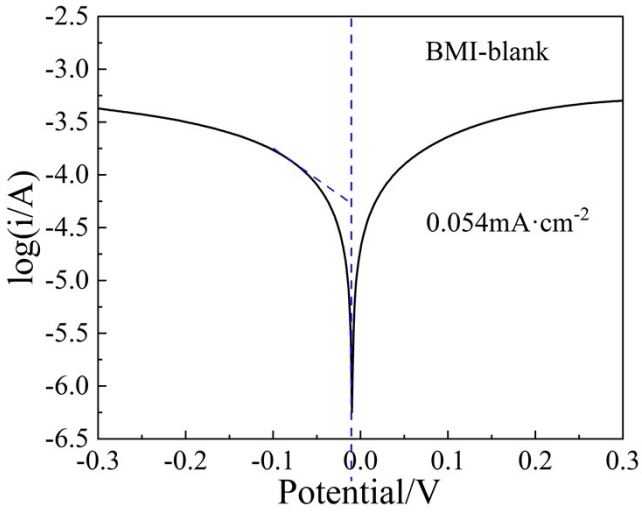

Figure S14. Tafel plots of symmetric Li|BMI-blank|Li cells

As shown in Figure S14, the exchange current densities of the Li|BMI-blank|Li is 0.054 mA cm^{-2}, much higher than that of Li|P_0-BMI-SCPE|Li, while lower than those of Li|$P_{2.5}$-BMI-SCPE|Li, Li|$P_{5.0}$-BMI-SCPE|Li and Li|P_{10}-BMI-SCPE|Li, indicating that the introduction of POSS significantly improves the interfacial compatibility between the electrolytes and lithium metal anodes.

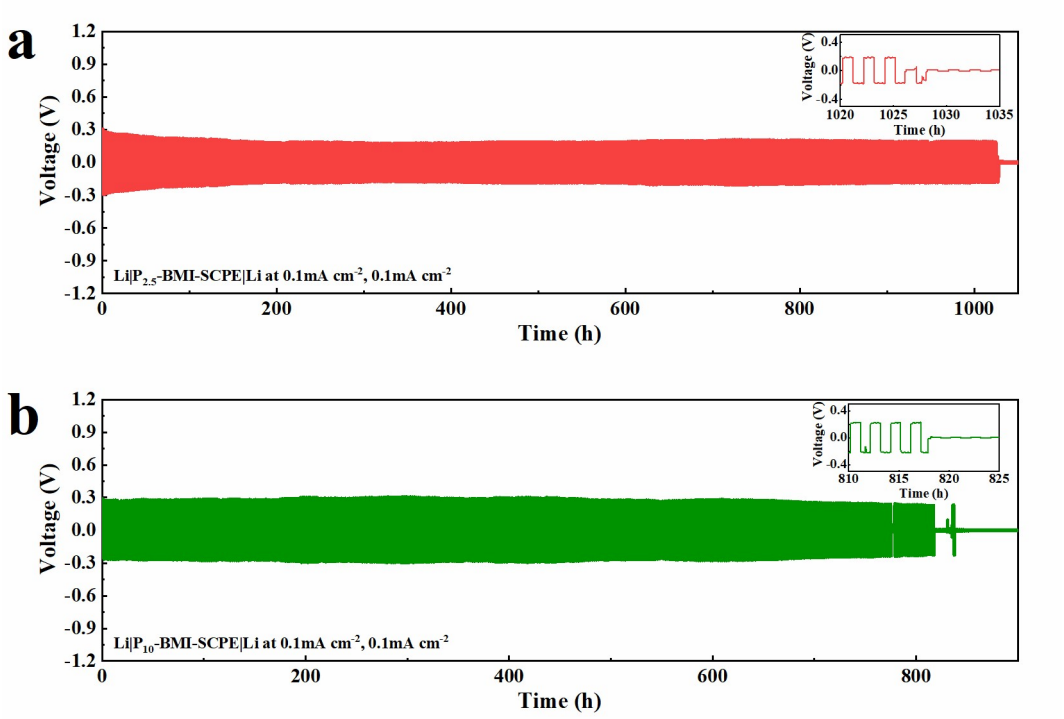

Figure S15. Galvanostatic cycling curves of (a) symmetric Li|P_0-BMI-SCPE|Li cells and (b) symmetric Li|P_5-BMI-SCPE|Li cells at room temperature with the current densities of 0.1 mA cm^{-2} for 0.1 mAh cm^{-2}, and enlarged view of the overpotential.

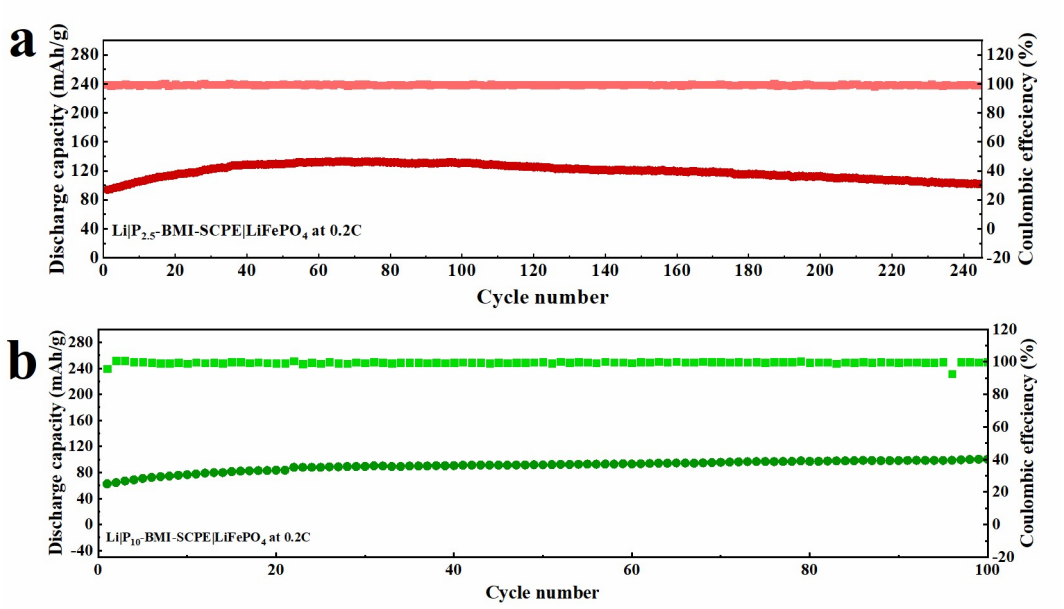

Figure S16. Cycle performances of (a) Li|$P_{2.5}$-BMI-SCPE|$LiFePO_4$ cells, (b) Li|P_{10}-BMI-SCPE|$LiFePO_4$ cells at a current density of 0.2 C, at 25 °C.

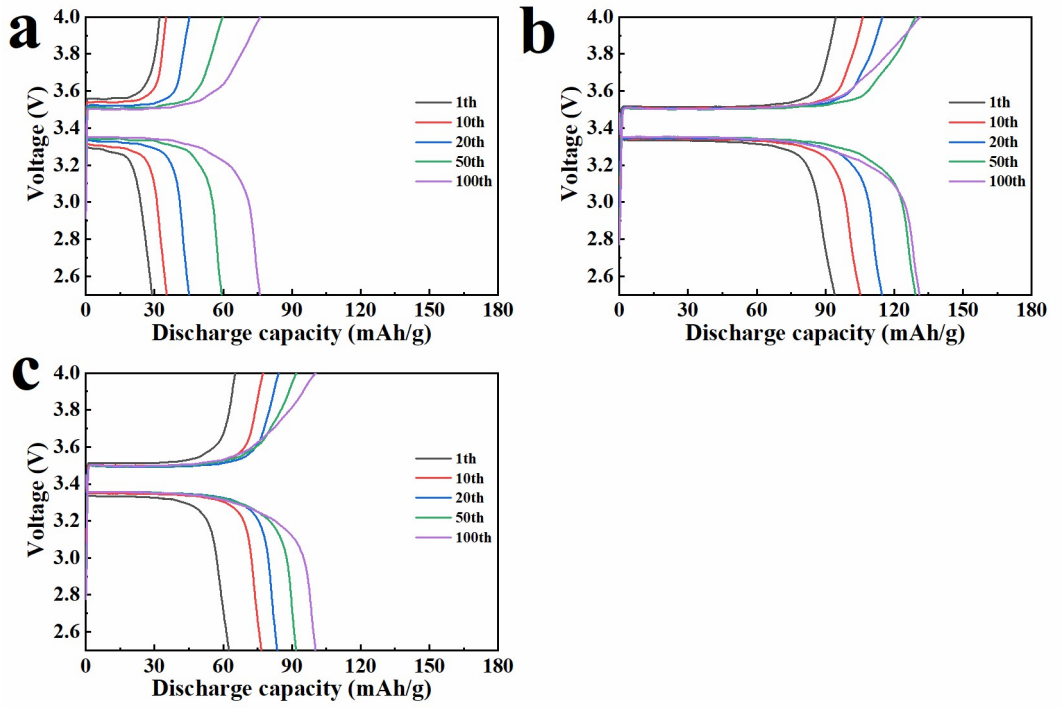

Figure S17. Charge and discharge curves of (a) Li|P_0-BMI-SCPE|$LiFePO_4$ cells, (b) Li|$P_{2.5}$-BMI-SCPE|$LiFePO_4$ cells, (c) Li|P_{10}-BMI-SCPE|$LiFePO_4$ cells at a current density of 0.2 C, at 25 °C

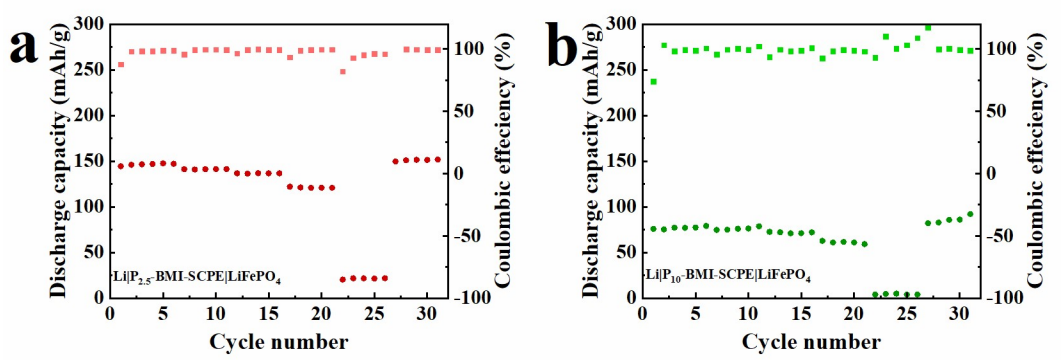

Figure S18. Rate performances of (a) Li|$P_{2.5}$-BMI-SCPE|$LiFePO_4$ cells, (b) Li|P_{10}-BMI-SCPE|$LiFePO_4$ cells at 25 °C

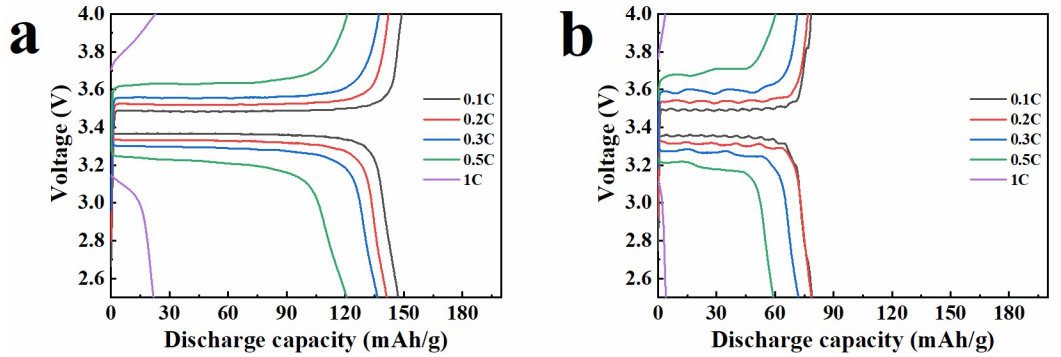

Figure S19. Charge and discharge curves of (a) Li|$P_{2.5}$-BMI-SCPE|$LiFePO_4$ cells, (b) Li|P_{10}-BMI-SCPE|$LiFePO_4$ cells at each rate at 25 °C